**NURETH14-557** 

# EXPERIMENTAL INVESTIGATION OF THE ACOUSTIC SOURCE LOCATION IN AN INLINE TUBE BUNDLE SUBJECT TO CROSS FLOW.

**S.L. Finnegan<sup>1</sup>, C. Meskell<sup>1</sup>** Trinity College, Dublin, Ireland

#### **Abstract**

The flow induced acoustics in an inline tube bank (P/d=3) subject to cross flow, indicative of a generic heat exchanger geometry, are examined over a range of flow velocities using Particle Image Velocimetry (PIV) coupled with acoustic analysis. In this way, the spatial and temporal aeroacoustic source distribution has been determined experimentally. It is found that the acoustic sources are most intense behind the first row due to the compactness of the vortices. However, a strong negative source (i.e. a sink) is also present in this location, so that the effect of the first row wake is actually to suppress the acoustic resonance. In subsequent rows, the sources are weaker and more dispersed, but the sink is reduced dramatically. The result is that after the first row the entire array contributes energy to the acoustic field.

#### Introduction

Acoustic resonance can occur when gas flow within a cavity or duct exhibits periodic vortex structures. If the frequency of flow periodicity is similar to an internal acoustic mode of the cavity, then a feedback can occur whereby energy is transferred from the flow into the acoustics, causing large pressure fluctuations. This acoustic resonance can lead to excess vibration and hence failure of components. This problem is well known is piping and pressure vessels, but is relatively unusual in nuclear reactor components, as often the working fluid is liquid. Indeed, in 2007 the US Nuclear Regulatory Commission, commenting on difficulties in the main steam line of a BWR during an uprating program, noted that "... recognition of acoustic resonance as causing adverse flow effects is relatively new to the nuclear power industry"[1]. Furthermore, in the Gen-IV roadmap it is recognized that additional research is required into acoustic resonance for helium systems envisaged in the Gas-cooled Fast Reactor (GFR) design[2]. This is also likely to be an issue for the Very High Temperature gas-cooled Reactor (VHTR).

Interaction between the resonant acoustic field and the unsteady flow field (flow-acoustic coupling) has been thoroughly investigated experimentally by, for example: Mohany and Ziada[3], Hall et al.[4], Fitzpatrick[5] and Finnegan et al.[6] for two tandem cylinders; and by Blevins and Bressler[7], and Oengören and Ziada[8-10] for tube arrays. While these studies have highlighted the mechanisms of acoustic resonance, they have not provided much empirical insight into the global distribution of acoustic sources in the flow field. Knowledge of the distribution of acoustic sources for a particular geometry of tube bundle could improve the design of a heat exchanger or possibly help improve acoustic resonance mitigation techniques. Furthermore, flow induced acoustic resonance is not completely understood, especially in complex geometries. This means that the conditions for the onset and the intensity of any resonance cannot be well predicted *a priori*. Nor can the effect of mitigation measures be easily assessed. Ideally, the compressible flow would be modelled so as to provide a predictive tool for the onset of lock-in, as well as the amplitude of the

acoustic resonance. However, while the field of computational aeroacoustics (CAA) is advancing rapidly, much of the research effort is focused on exterior flows. Furthermore, simulation of the coupled fluid flow and acoustic systems in the complex geometry of a heat exchange system appears to be some way off.

In this context, the current work attempts to provide a rich data set for a reference configuration which can be used as an interim validation of simulation tools, while also providing some physical insight into the mechanism of acoustic resonance in tube bundles. The paper outlines the basic analysis approach and the experimental procedure before presenting the key results of the study.

### 1. Methodology for calculating the instantaneous aeroacoustic energy.

Experimental method used to calculate the spatial distribution of the acoustic energy has previously been developed for arrangements of two and four cylinders[6, 11]. The basic approach is based on a formulation developed by Howe[12] (see Eqn. 1) which calculates the dissipation of acoustic energy from the sharp edges of a rigid boundary by the generation of vorticity in a low sub-sonic mean flow with uniform density and is an extension of his theory of vortex sound[13].

$$\Pi = -\rho \int_{R} \omega \cdot (V \times U_a) dR \tag{1}$$

This equation was derived from the kinetic energy of the incompressible velocity field in a divergence-free, isentropic mean flow. It predicts that the acoustic power flux of the vortical structures is equal to the rate at which work is performed by the Coriolis force density experienced by the vortical structures[12]. In fact, Eqn. 1 states that acoustic energy generated over an entire acoustic wave cycle can be calculated from integral of the triple product between the vorticity vector  $\boldsymbol{\omega}$ , the local hydrodynamic flow velocity vector  $\boldsymbol{V}$  and the acoustic particle velocity vector  $\boldsymbol{U}_a$ , where  $\rho$  is the mean density of air and  $\boldsymbol{R}$  is the control volume. Figure 1 shows the conceptual approach used to resolve the three components of Eqn. 1. A central assumption is that the hydrodynamic and acoustic components in the flow field can be decoupled from each other, resolved separately and then re-coupled to calculate the acoustic sources. This requires a low Mach number.

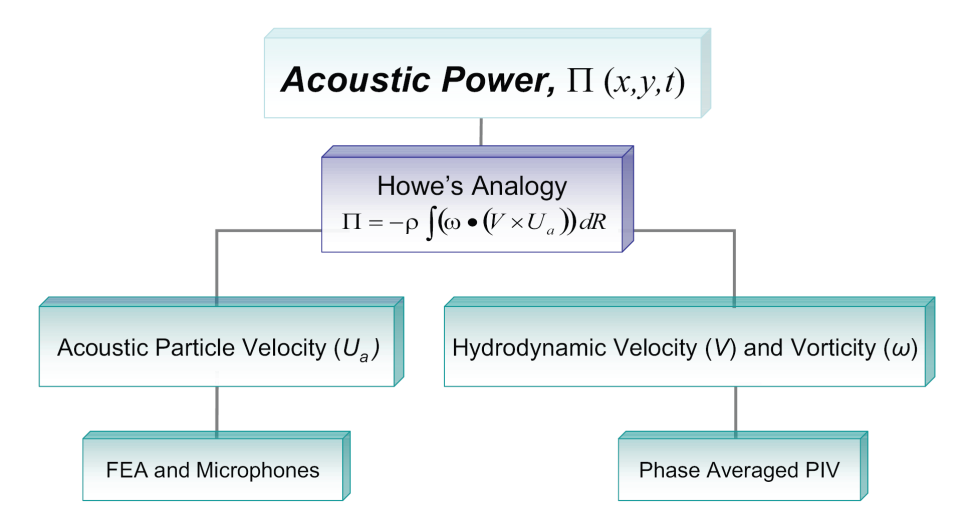


Figure 1 Conceptual strategy to resolve the components of Howe's Analogy (Eqn 1).

#### 2. Experimental facility.

The target geometry was a four row inline square tube array (P/d=L/d=3.0). The tube diameter, d, was 13mm. Tests were conducted in a small scale, draw down wind tunnel with a test section of 125mm x125mm. Figure 2(a) shows a schematic of the experimental geometry. The position of the roving hotwire probe and fixed reference microphone are shown as HW2 and M1 respectively. Note that side branches were added to reduce the resonant acoustic frequency,  $f_a$ =329 Hz. The side branches are sufficiently wide that the acoustic mode shape only differs from what would be expected in an infinite array in a straight duct at the four corner locations in the array. Many aspects of the setup are similar to previous test campaign with two tandem cylinders[6]. Further details can be found in Finnegan's thesis[14] The tube array spacing is larger than would be expected in nuclear installations. In fact it is classified as "large" streamwise spacing ratio according to Oengören and Ziada[9]. This large spacing was chosen to facilitate PIV measurements. However, it should be remembered that the current test campaign is intended to provide validation data for a reference case, rather than target a particular operational design.

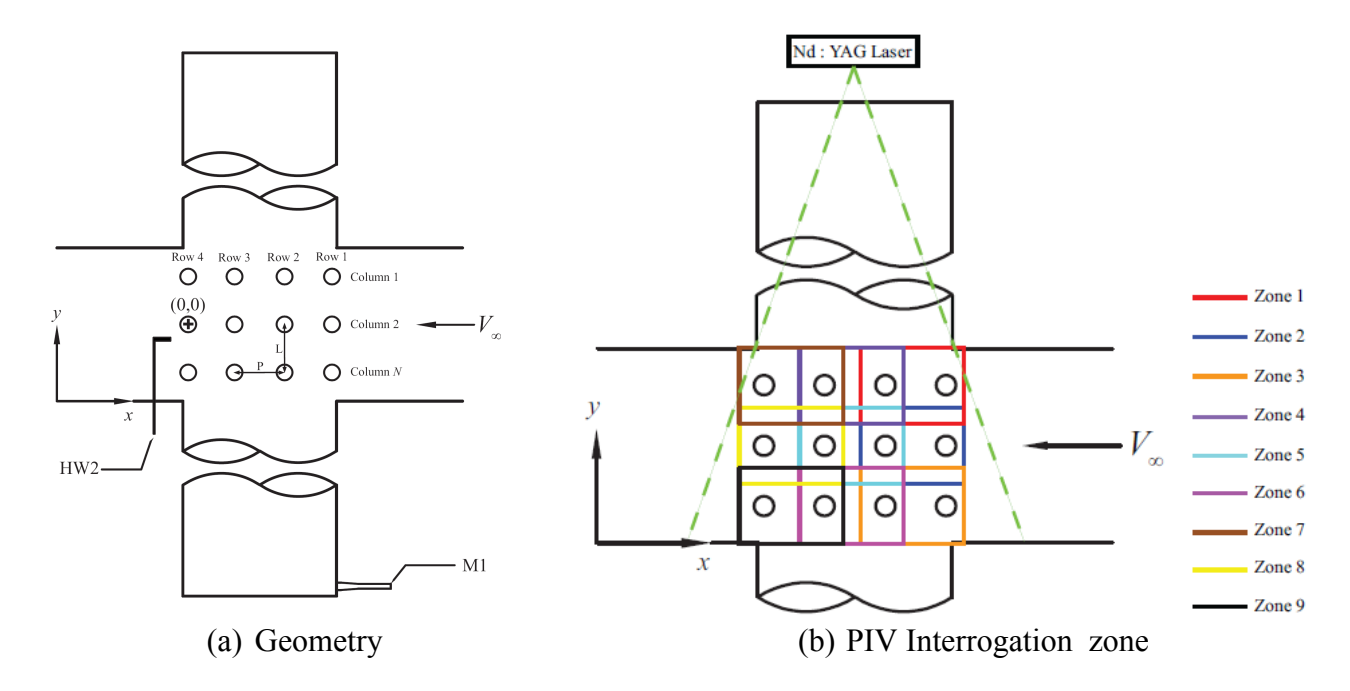


Figure 2 Schematic of experimental setup.

Sound pressure was monitored using a flush mounted G.R.A.S. Type 40BH microphone and location M1. The hotwire and the microphone data was digitized using an NI PXI 4472B data acquisition card. The seeding particles of diethyl-hexylsebacate (DEHS) with a diameter of approximately 1 $\mu$ m were illuminated by a Nd:YAG pulsed laser. A Davis Flowmaster 3 CCD camera was used to capture the PIV images and the PIV post processing was completed with LaVision DAVIS 7.2. In order to maintain sufficient spatial resolution to ensure good quality vector maps, which are unbiased by peak locking, the field of view of the PIV had to be restricted to 50mm x 40mm. As a result, the entire array was decomposed into 9 overlapping zones, shown in Figure 2(b). Data for each zone was phase locked to the microphone signal and ensemble averaged, allowing a composite velocity map of the entire array to be obtained.

#### 3. Flow-acoustic coupling.

Figure 3 shows the aeroacoustic response of this tube array configuration. Figure 3(a) shows the acoustic pressure measured with microphone M1 whilst Fig. 3(b) shows a waterfall plot of the streamwise velocity spectra measured by the hotwire HW2. Acoustic excitation is triggered by vortex shedding at acoustic-Strouhal coincidence. The increase in acoustic pressure is gradual as  $f_v$  approaches  $f_a$  but accelerates at acoustic-Strouhal coincidence. Hence this square array would be classified as experiencing coincidence resonance. The system remains "locked-in" for roughly 4 m/s. When "lockin" is broken, the vortex shedding frequency  $f_v$  jumps up to a higher frequency and increases with flow velocity. However, at these higher velocities, the vortex shedding gradually diminishes into broadband turbulent structures. This is apparent in the waterfall plot as the strength of the Strouhal-dependency after "lock-in" is much lower compared to the dependency before "lock-in". Closer inspection of the waterfall plot reveals that the  $f_v$  suddenly jumps to a higher frequency at  $V_{\infty} = 14$  m/s and follows a slightly different Strouhal dependency before "lock-in" occurs. This occurs at approximately the same velocity as the onset of the acoustic pressure increase in Figure 3(a). This may represent the switch between global jet instability excitation and local wake instability excitation discussed by Ziada and Oengören[9]. The frequencies before the jump yield a Strouhal number based on gap velocity of  $St_g$  = 0.14 while the frequencies after the jump yield a Strouhal number of  $St_g = 0.15$ . Ziada and Oengören[9] reported Strouhal numbers of 0.14 and 0.16 respectively in their water tunnel tests.

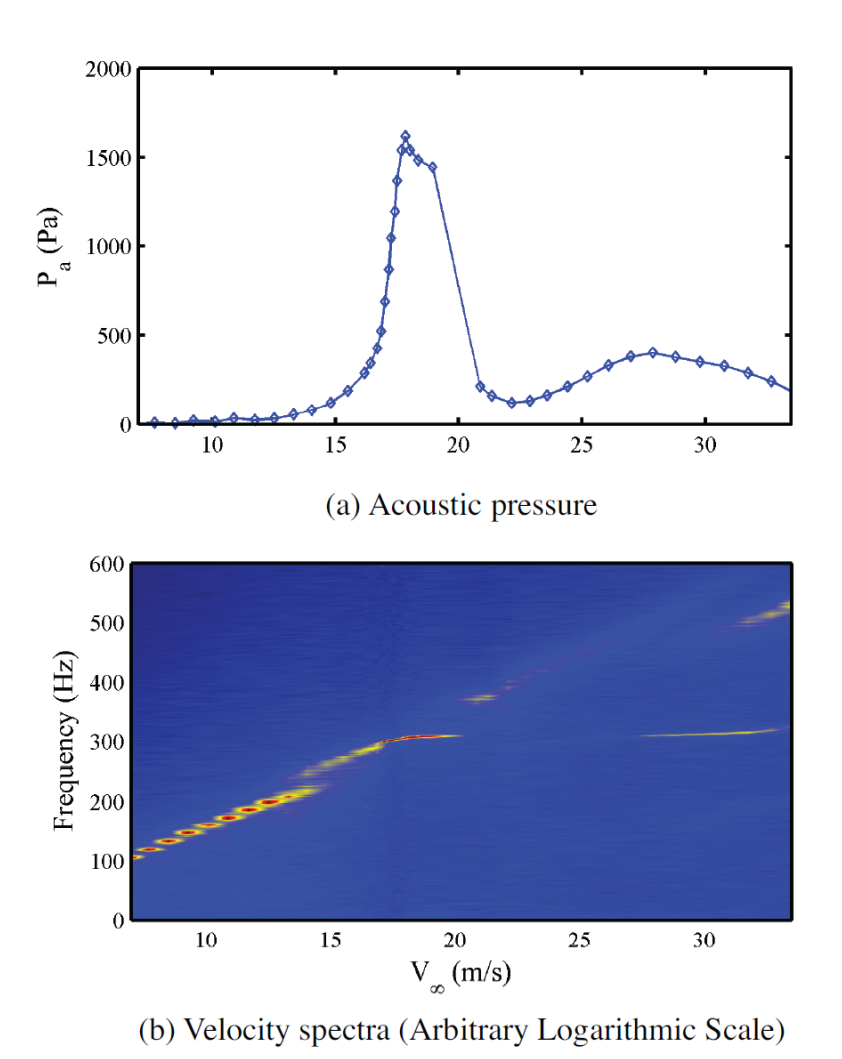


Figure 3 Aeroacoustic characteristics measured by microphone M1 and hotwire HW2.

#### 4. Spatial distribution of acoustic power.

As discussed above, in order to resolve the entire flow field, the setup was decomposed into 9 zones, the nature of the phase locked PIV measurement means that testing and postprocessing is very time consuming. For this reason, the full field acoustic power was investigated for only one flow velocity ( $V_{\infty} = 18.2 \text{ m/s}$ ;  $V_g = 27.8 \text{m/s}$ ) which corresponded to acoustic–Strouhal coincidence. The pressure measured by microphone M1 at acoustic-Strouhal coincidence was  $P_a = 1376 \text{ Pa}$  (156.75 dB) which meant that the dimensionless acoustic particle velocity was  $U_a/V_{\infty} = 0.18$ ;  $U_a/V_g = 0.12$ .

Triggered PIV acquisition, enabled phase locked ensemble averaging. The microphone signal was used as a time reference. The velocity field was resolved using 100 image pairs, at phase increments of  $22.5^{\circ}$ . Thus the acoustic cycle was resolved with 16 full field maps. When the net acoustic power at all 16 phases are examined, is found that maximum acoustic power is generated at  $\phi = 22.5^{\circ}$  and  $\phi = 202.5^{\circ}$ , while at  $\phi = 112.5^{\circ}$  and  $\phi = 292.5^{\circ}$  acoustic power is absorbed. Figure 4 plots the vorticity and the corresponding acoustic power calculated using Eqn. (1) at  $\phi = 22.5^{\circ}$ ,  $\phi = 112.5^{\circ}$ ,  $\phi = 202.5^{\circ}$ ,  $\phi = 292.5^{\circ}$ . Each tube exhibits a white "halo". In this region there is no data available because of parallax; the tubes themselves obscure the view of the flow field adjacent to the surface.

Inspection of the vorticity plots in Fig. 4(a) show that well defined vortices form from the first row of cylinders, propagate in the wake and impinge onto the second row. The vortices formed from one shear layer are out-of-phase with the vortices formed in the adjacent shear layer of the neighbouring column. As the vortex impinges, it induces a second, weaker vortex to form from the second row. This vortex forms on the other side of the cylinder from which the impinging vortex was shed and so has opposite polarity. The shedding of this second vortex is timed with the shedding of a strong vortex of similar sense from the first row. That is to say, the structures are highly synchronised across the bundle. The vortices formed in the second row are spread out over a larger area than the vortices shed from the first but have a smaller magnitude. Moreover, they also seem to be less coherent. When the vortices formed from the second row impinge on the third row, even less coherent vortices form in their wake. At this stage, the flow has become mostly turbulent which is apparent from the noisy vorticity contours. Even though the structures in the deeper rows are less defined and much more turbulent compared to upstream rows, they continue to form alternatively in the wakes of the cylinders and synchronisation of the flow seems to remain between both the rows and the columns. The structure of the phased averaged flow field agree well with the findings of Ziada and Oengören[9].

Figure 4(b) shows the acoustic power at each phase. Much stronger sources and sinks are generated at phase of  $22.5^{\circ}$  and  $202.5^{\circ}$  compared to  $\phi = 112.5^{\circ}$  and  $\phi = 292.5^{\circ}$  because the magnitudes of the acoustic particle velocities (negative and positive) are much greater at  $\phi = 22.5^{\circ}$  and  $\phi = 202.5^{\circ}$  than at  $\phi = 112.5^{\circ}$  and  $\phi = 292.5^{\circ}$ . Concentrating on the phases that generate acoustic power first, inspection of Fig. 4 reveals that the sources generated at  $\phi = 22.5^{\circ}$  correspond to structures shed from the top sides of the cylinders whilst sources generated at  $\phi = 202.5^{\circ}$  correspond to structures shed from the bottom sides of the cylinders. One can see that at both of these phases, the vortices are still developing behind rows 1 and 2 and have not quite fully formed. They have a significant contribution to Eqn. (1) because they possess a high level of vorticity due to their attachment to the shear layer. On the other hand, for the phases that absorb acoustic power, it can be seen that the sinks generated at  $\phi = 112.5^{\circ}$  correspond to structures shed from the top sides of the cylinders whilst sinks generated at  $\phi = 292.5^{\circ}$  correspond to structures shed from the bottom sides of the cylinders. One can see that at both of these phases, the vortices (which were previously still forming) are now fully developed and just about to impinge on a downstream cylinder. Even though the acoustic particle velocity at these phases has a reduced influence on Eqn. (1), the fact that the vortices are fully developed and cover a large area means their

contribution is still significant and hence absorption occurs. It seems that the generation of acoustic power in this inline tube bundle is due to the generation and formation of new structures from the cylinders whilst the absorption of acoustic power seems to be due to their interaction with a downstream cylinder in the wake.

The spatial distribution of the net acoustic energy per cycle generated by the tube bundle can be seen in Fig. 5. It should be noted that due to parallax, there is a substantial portion of the flow field for which there is no information available; these areas appear as white voids in Fig. 5. The result is that while the spatial distribution of time averaged acoustic power offers quantitative information locally, only qualitative information is available globally. Nonetheless, some useful observations can be made. The generation/absorption of acoustic energy occurs in a periodic fashion from the first row of the array to the last. Moreover, the distributions of the sources and sinks around each column are almost identical, at least for the first three rows. The generation of acoustic energy seems to be largely due to the formation of vortices behind the first and second rows, whilst the absorption of energy seems to be due to the vortices impinging on the cylinders. Fitzpatrick and Donaldson[15] concluded that vortex shedding from the first few rows of a shallow inline tube bundle (no. rows < 5) is the primary source of acoustic resonance. Indeed, the region near the second row seems to be particularly important as there are very large sinks situated just before it and very strong sources situated just aft of it. The sinks just in front of the second row cylinders have the strongest magnitudes of all the structures. The first and second rows have the strongest sources and sinks as they have the best defined hydrodynamic structures. However, as can be seen, the less defined turbulent structures behind the third row are significant in the generation of acoustic power. A general observation is that the strength of the sources/sinks decreases from row to row. This is not thought to be due to the drop off in the acoustic particle velocity but rather to the breakdown in coherent vortex structures as the flow travels deeper into the array. In fact, the net contribution in each inter-cylinder gap is comparable, so that, although the strongest acoustic sources are without doubt to be found between row 1 and 2, the entire array contributes significantly to the generation of sound.

# 5. Comparison with two tandem cylinders.

The coupled flow-acoustic resonance of two tandem cylinders in a duct has been extensively studied in the literature, and is reasonably well understood. In order to build on this knowledge base, Figure 6 compares the normalised net acoustic energy transfer at a streamwise location per cycle  $E^*$  (as a function of the distance from the upstream cylinder) generated around the cylinders in column 2 of the array with that generated by the two tandem cylinders with pitch ratio (P/d) of 2.5 during precoincidence resonance[6]. Note that the reduced velocities are similar in these two cases. The normalised energy  $E^*$  was defined by Finnegan et al.[11] as:

$$E^* = \frac{E}{P_a d} \tag{2}$$

where E is net acoustic energy at a stream-wise location, per unit tube span, per cycle,  $P_a$  is the sound pressure level, and d is the cylinder diameter. The distributions of the sources and sinks between the two cases are remarkably similar suggesting that the mechanisms generating and absorbing acoustic power are similar. As can be seen, the strongest sinks form at x = -2.5d for the tandem cylinder case and at x = -2.2d for the tube bundle. The biggest difference between the two plots is the relative magnitudes of the sources and sinks in the wake of the first row. This is due to the extra stream-wise spacing between the cylinders for the inline tube bundle. For the tandem cylinder configuration, the downstream cylinder is located at x = -2.5d and the vortices in this are stretched by the downstream cylinder. Hence, they are not developing or strengthening. For column 2 of the inline tube bundle, the cylinder in the second row is at x = -3d which means the vortices can still grow and strengthen. The

# The 14<sup>th</sup> International Topical Meeting on Nuclear Reactor Thermalhydraulics, NURETH-14 Toronto, Ontario, Canada, September 25-30, 2011

added space has afforded the vortex more time to develop which is why it has a stronger contribution. For the two tandem cylinder case, it was found that pre-coincidence acoustic resonance is generated by the formation of vortices in the gap between the two cylinders and that absorption of acoustic power is related to the impingement of the vortices on the downstream cylinder. This is largely the case here. However, it is interesting how changing the spacing of the gap between two cylinders by only a small amount can drastically change the relative contribution of the sources and sinks. Finnegan et al.[11] reported a similar effect for a four cylinder configuration with a pitch ratio P/d = 3.

As previously mentioned, the effect of parallax will be to make the acoustic power in the region of the tubes uncertain, and so the net acoustic power for the entire system does not give a reliable metric of whether the system would tend to be locked in. This problem will not be present in numerical simulations, which can be validated against the local spatial distribution of acoustic power measured in this paper.

#### 6. Conclusions.

The most general conclusion to be drawn is that the combined PIV, FEA and microphone approach, previously applied to tandem and four cylinders, is applicable to the geometrically more challenging configuration of a tube array, although the practical obstacles to overcome in implementing the experimental protocol are significant.

Nonetheless, detailed information has been obtained for a square inline array with a pitch ratio of 3.0 at acoustic-Strouhal frequency coincidence. The behaviour of the array is broadly consistent with that of similar geometry reported in the literature. The principal physical insights to be gained in this study are:

- The flow structure between the first three rows of the array during "lock-in" is highly synchronous despite its geometric complexity and moderate Reynolds number.
- The mechanisms of acoustic resonance for the tested array are similar to those observed in the tandem cylinder and four cylinder configurations previously reported.
- Vortex shedding in the wake of the first and second rows provide the dominant sources in the flow field. The strength of the sources diminishes with each row as the vortex structures become less coherent. However, the net sound generated by these relatively diffuse structures is not insignificant.
- The absorption of acoustic resonance in this particular array is largely associated with the vortices shed from the first row of cylinders impinging on the second row. The large streamwise spacing allows more time for the vortices to develop which means their contribution will be more significant.

The effect of parallax means that there are gaps in the data at important locations in the field. However, the data provides a useful reference case which will allow deep validation of any numerical simulation of flow-acoustic resonance in tube arrays.

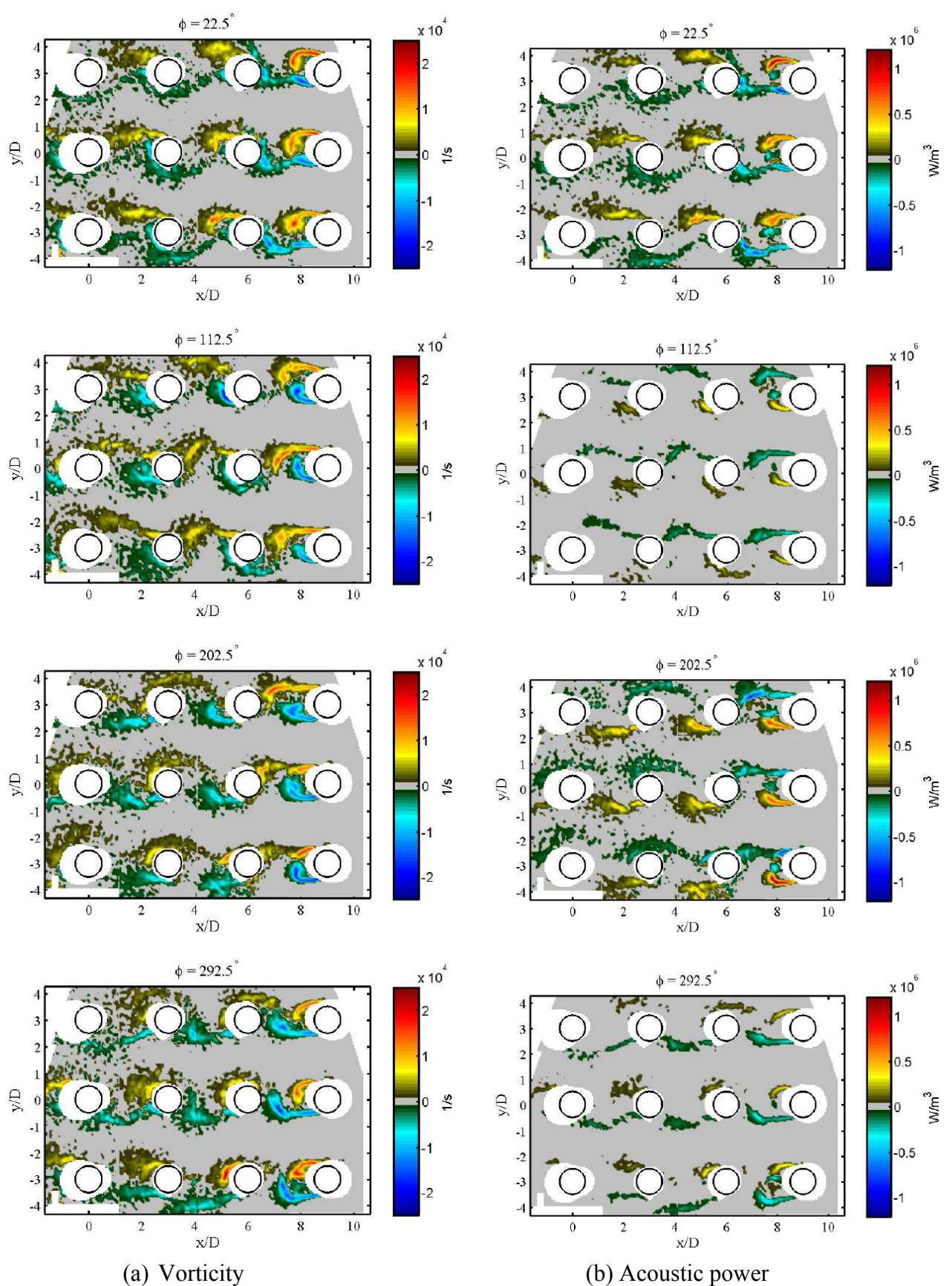


Figure 4 The full field hydrodynamic vorticity and acoustic power for different phases in the acoustic wave cycle at acoustic-Strouhal coincidence,  $f_a = 311$  Hz and  $U_a/V_\infty = 0.18$ .

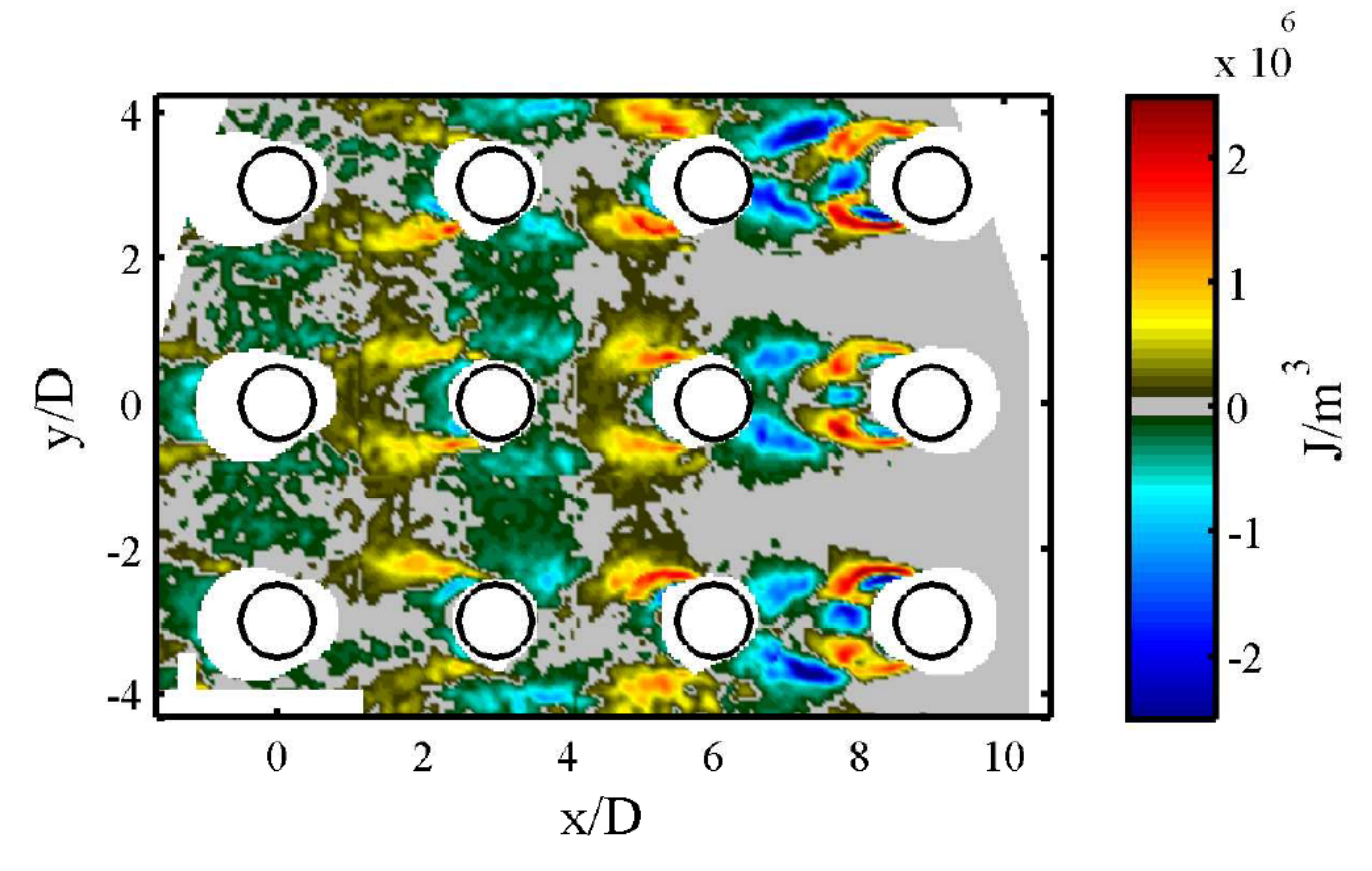


Figure 5 The total acoustic energy per cycle generated at acoustic-Strouhal coincidence.

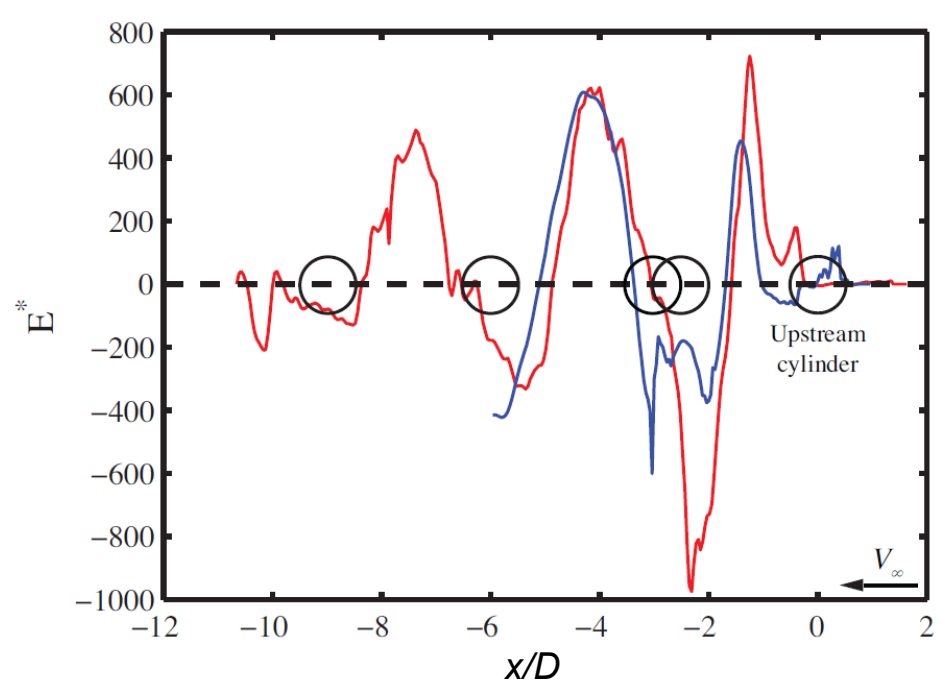


Figure 6 Comparison of normalized acoustic energy per cycle  $E^*$  as a function distance from the first upstream cylinder: — Inline tube bundle (P/d = 3), current study; — two tandem cylinders during pre-concidence resonance (P/d = 2.5) from Finnegan et al.[6]

## 7. References

- 1. Reyes, L.A., *Power Uprate Program Status Report SECY-07-0090*. 2007, U.S. Nuclear Regulatory Commission.
- 2. *A Technology Roadmap for Generation IV Nuclear Energy Systems*. 2002, U.S. DOE Nuclear Energy Research Advisory Committee and the Generation IV International Forum.
- 3. Mohany, A. and S. Ziada, *Flow-excited acoustic resonance of two tandem cylinders in cross-flow*. Journal of Fluids and Structures, 2005. **21**(1).
- 4. Hall, J.W., S. Ziada, and D.S. Weaver, *Vortex-shedding from single and tandem cylinders in the presence of applied sound.* Journal of Fluids and Structures, 2003. **18**(6): p. 741-758.
- 5. Fitzpatrick, J.A., *Flow/acoustic interactions of two cylinders in cross-flow*. Journal of Fluids and Structures, 2003. **17**: p. 97-113.
- 6. Finnegan, S.L., C. Meskell, and S. Ziada, *Experimental Investigation Of The Acoustic Power Around Two Tandem Cylinders*. Journal of Pressure Vessel Technology, 2010. **132**: p. 041306 (12 pp.).
- 7. Blevins, R.D. and M.M. Bressler, *Experiments on acoustic resonance in heat exchanger tube bundles*. Journal of Sound and Vibration, 1993. **164**: p. 502-534.
- 8. Oengoren, A. and S. Ziada, *An in-depth study of vortex shedding, acoustic resonance and turbulent forces in normal triangle tube arrays.* Journal of Fluids and Structures, 1998. **12**: p. 717-758.
- 9. Ziada, S. and A. Oengoren, *Vorticity shedding and acoustic resonance in an in-line tube bundle Part I: Vorticity shedding.* Journal of Fluids and Structures, 1992. **6**: p. 271-292.
- 10. Oengoren, A. and S. Ziada, *Vorticity shedding and acoustic resonance in an in-line tube bundle Part II: Acoustic resonance*. Journal of Fluids and Structures, 1992. **6**(293-309).
- 11. Finnegan, S.L., P. Oshkai, and C. Meskell. *Experimental methodology for aeroacoustic source localisation in ducted flows with complex geometry*. in *16th AIAA/CEAS Aeroacoustics Conference (31st AIAA Aeroacoustics Conference), June 7, 2010 June 9, 2010*. 2010. Stockholm, Sweden: American Institute of Aeronautics and Astronautics Inc.
- 12. Howe, M.S., *Dissipation of sound at an edge*. Journal of Sound and Vibration, 1980. **70**: p. 407-411.
- 13. Howe, M.S., Contributions to the theory of aerodynamic sound, with application to excess jet noise and the theory of the flute. Journal of Fluid Mechanics, 1975. 71: p. 625-673.
- 14. Finnegan, S.L., *Resonant Aeroacoustic Source Localisation In Ducted Bluff Body Flows*, in *School of Engineering*. 2011, Dublin University: Dublin. p. 247.
- 15. Fitzpatrick, J.A. and I.S. Donaldson, *A Preliminary Study of Flow and Acoustic Phenomena in Tube Banks*. ASME Journal of Fluids Engineering, 1977. **99**(4): p. 681-686.